Deposition velocity of inertial particles driven by wall-normal external force in turbulent channel flow

Pinzhuo Chen [1], Sheng Chen [1,*], Tianyi Wu,[1] Xuan Ruan [2], and Shuiqing Li [2]

[1]*State Key Laboratory of Coal Combustion, School of Energy and Power Engineering, Huazhong University of Science and Technology, Wuhan 430074, China*

[2]*Key Laboratory for Thermal Science and Power Engineering of Ministry of Education, Department of Energy and Power Engineering, Tsinghua University, Beijing 100084, China*

We perform a point-particle Lagrange simulation to investigate the effect of the wall-normal external force and the particle inertia on the clustering and deposition of particles in wall-bounded turbulence. It is found that the mean slip velocity of particles in the outer layer equals the production of the Stokes number (St) and a dimensionless force parameter (ψ). The first-time collision velocity of particles when they impact the wall is recorded and the mean deposition velocity $\langle v_d \rangle$ is compared with the mean slip velocity in the outer layer. An anomalous enhancement of $\langle v_d \rangle$ is reported and the relative velocity increment, $\langle v_d \rangle / (\mathrm{St}\psi) - 1$, shows an increasing-decreasing trend as the Stokes number increases. The largest enhancement of the deposition velocity is observed for particles with moderate inertia due to (1) the preferential distribution of particles in the near-wall high-velocity regions and (2) the insufficient deceleration of inertial particles in the viscous sublayer. Given a strong wall-normal force, the clustering of particles is inhibited, leading to a decline in the relative velocity increment. Finally, we show that the deposition velocity resembles the terminal velocity in a stationary fluid when the particle relaxation length is considerably smaller than the thickness of the viscous sublayer.

I. INTRODUCTION

The deposition of particles in wall-bounded turbulent flows is prevalent in natural phenomena and industrial applications. Typical examples include the sand sedimentation in rivers [1,2], the removal of aerosol particles in electrostatic precipitators (ESPs) [3], the deposition of particles in gas turbines [4], and the fouling of heat exchangers [5]. In most practical scenarios, particles experience external forces, such as the gravitational force, electrostatic forces, and thermophoretic force [6,7]. Due to the inhomogeneity and multiscale characteristics of the flow structures, predicting the deposition velocity of particles in turbulent channel flows is highly challenging. The decorrelation of particle motions from the fluid caused by the particle inertia and external forces gives rise to additional complexity [8].

In the absence of external forces, inertial particles in wall-bounded turbulence tend to accumulate in a thin layer in the vicinity of the wall. This phenomenon is known as turbophoresis [9]. The turbophoresis effect leads to the inhomogeneous distribution in the wall-normal direction [7–11]. The particle migration rate is found to be proportional to the gradient of the wall-normal particle velocity variance [10]. Marchioli and Soldati [12] confirmed that the sweep and ejection events with substantial spatial coherence in the near-wall region are the governing mechanism to drive the

* sheng_chen@hust.edu.cn

particle move to or away from the wall. The existence of the rear end of the quasistreamwise vortices prevents the transport of particles away from the wall by ejections and results in the accumulation of particles in the near-wall region. In wall-bounded turbulence, particles with Stokes number of the order of unity are concentrated into longitudinal bands in the low-speed streaks, while larger particles tend to distribute more randomly, indicating that the clustering is strongly related to the particle inertia [13]. Furthermore, the angular distribution function (ADF) is used to quantify small-scale clustering and found that the clustering is most significant within the range of the viscous Stokes number $St^+ = 10-50$ [11]. Recently, it is found that the scale of particle streaks increases with the friction Reynolds number Re_τ and even heavy particles ($St^+ = 150$) can form large-scale clustering streaks at $Re_\tau = 1000$ [14].

When applying a wall-normal external force, the spatial distribution of particles will be significantly influenced [15–18]. The gravitational force applied in the wall-normal direction intuitively increases the particle concentration in the lower part of the channel, especially in the vicinity of the wall, when the boundary condition with elastic particle-wall collisions is applied. The particle distribution can be strongly modified by gravity-induced settling even when the force magnitude is extremely small [15]. Lee and Lee [19] adopted a direct numerical simulation of the turbulent channel flow laden with heavy particles and found that, under the gravitational force, the preferential sweeping effect occurs in the near-wall region when the Kolmogorov scale Stokes number is around unity. In contrast, heavy particles with $St \gg 1$ deposit on the wall without clustering in low-speed streaks. Under the combined effect of shear turbulence and gravity, the cluster shows a preferential direction which aligns more with the horizontal direction than nongravity conditions [20]. In the net sedimentation conditions under gravity, the self-similarity of the geometries of particle clusters is observed in the log-law layer; the probability density functions of the particle cluster area can be characterized by the $-5/3$ power law [21].

In practical scenarios, particle dynamics can be affected by other driven forces, such as the electrostatic forces in ESP and the thermophoretic forces in gas-solid reactors with a temperature gradient. When coupling with the turbulent effect, these external forces can lead to significant modifications of the spatial distribution of particles [12,22–25]. Recently, it has been reported that applying an alternating current electric field across the channel walls can suppress the turbophoresis of charged particles, decreasing the near-wall concentration of particles by up to two orders of magnitude [7].

The velocity of particles when they collide with the wall (also known as the deposition velocity) is a key parameter that would affect the postcollision behavior (either sticking or rebound) of particles and has been widely investigated with or without external forces [26–30]. In the absence of the external force, depositing particles can be divided into two populations: the free-flight particles, which are entrained into sweep regions and get enough momentum to deposit with large wall-normal impact velocities, and the diffusional deposition population with negligible wall-normal deposition velocities [31–33]. Particles in the free-flight population obtain a relative high wall-normal momentum from the turbulence and then cross the quiescent viscous sublayer and hit the wall. The free-flight mechanism becomes more remarkable when the particle inertia increases. The diffusional deposition, which is induced by residual turbulent fluctuations in the near-wall regions, dominates the deposition of light particles [31–34].

Theoretical models and empirical correlations have been proposed to predict the deposition velocity for particles considering the combined effect of driven forces, Brownian diffusion, turbulent diffusion, and particle inertia [26–30,35,36]. The mean particle velocity is formulated based on the phase-space probability density of the particle velocities and positions [37]. The proposed expression can evaluate the contributions from different mechanisms, e.g., inertia-based diffusion, the turbophoretic drift [38,39], the Stokes settling, and the preferential sampling [11,40], to the wall-normal velocity of inertial particles. The mean wall-normal particle velocity in wall-bounded turbulence evidently exceeds Stokes settling velocity in quiescent flow [18]. When particles are sufficiently far from the wall, the velocity enhancement is due to the preferential sweeping. When particles are close to the wall, the settling velocity is governed by the turbophoretic drift [37].
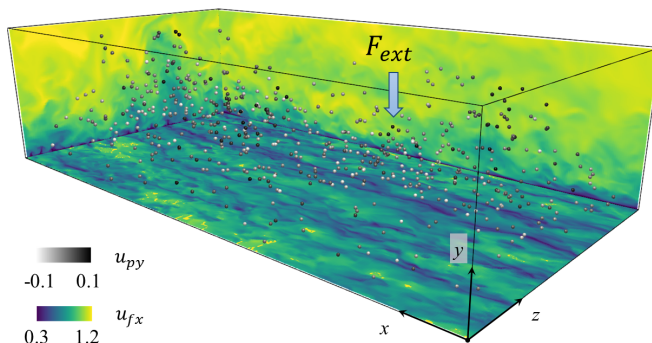
FIG. 1. Snapshot of the simulated system. The particles and the flow field are colored according to the wall-normal velocity (u_{py}) and streamwise velocity (u_{fx}), respectively.

Previous studies mainly focus on the influence of particle inertia without varying the magnitude of the driving force. It is unclear to what extent the external force affects particle deposition velocity. Intuitively, a strong external force can drive the particles off the streamlines even when the particles have negligible inertia. It affects the clustering of particles in the coherent near-wall flow structures, which can have further impact on the deposition velocity of particles (both the free-flight population and diffusional deposition population). Moreover, previous studies mainly considered the mean wall-normal particle velocity. There have been few reports of high-order statistics of the particle velocity and the fluid velocity at the particle position.

Motivated by the question above, we perform direct numerical simulation (DNS) to track point particles with different inertia in the presence of a uniform external force, which is varied over a wide range. The computational setup, the numerical model, and its validation will be given in Sec. II. A statistical description of the particle deposition velocity is presented in Sec. III A, where an anomalous enhancement of the deposition velocity is found for particles with moderate inertia. To explain this phenomenon, the roles of the external force and turbulent structures on the clustering in the near-wall regions are discussed in Sec. III B, and the particle deceleration process in the boundary layer is discussed in Sec. III C. In Sec. IV, we summarize our conclusions and give questions for future study.

II. COMPUTATIONAL SETUP AND MODEL VALIDATION

We consider the transport of spherical non-Brownian point particles in a turbulent channel flow. The flow field is obtained from the Johns Hopkins Turbulence Databases (JHTDB) [41–43], which is produced from the direct numerical simulation (DNS) of a wall-bounded channel flow by solving Navier-Stokes equations.

$$\nabla \cdot \boldsymbol{u}_f = 0, \tag{1a}$$

$$\frac{\partial \boldsymbol{u}_f}{\partial t} + \boldsymbol{u}_f \cdot \nabla \boldsymbol{u}_f = -\frac{1}{\rho_f} \nabla p + \nu \nabla^2 \boldsymbol{u}_f, \tag{1b}$$

where $\boldsymbol{u}_f$ denotes the flow velocity vector, p denotes the hydrodynamic pressure, ρ_f is the fluid density, and ν is the kinematic viscosity. The equations are solved by a Fourier-Galerkin pseudospectral method in the x and z directions and a seventh basis-splines collocation method in the wall-normal (y) direction. Time integration is implemented by a third-order Runge-Kutta method and the flow data within the time span $t \in [0, 25.99]$ is stored in JHTDB with a time step $\delta t = 0.0065$.

As shown in Fig. 1, the size of the computational domain is $(L_x, L_y, L_z) = (8\pi h, 2h, 3\pi h)$, in the streamwise ($x$), spanwise ($z$), and wall-normal ($y$) directions, respectively. The no-slip boundary condition is set at the walls ($y = 0$ and $y = 2h$) and the periodic boundary condition is applied in

the spanwise (z) and streamwise (x) directions. Since we focus on the first-time collision of particles with the wall in the current work, particles are removed from the computational domain upon wall collisions. The wall-normal collision velocity, which is also known as the deposition velocity, is termed as v_d.

The computational domain is discretized into $N_x \times N_y \times N_z = 2048 \times 512 \times 1536$ grid nodes with a uniform grid spacing $\Delta x = 0.0123$ and $\Delta z = 6.3 \times 10^{-3}$ in the x and z directions. In the wall-normal direction, the grid spacing ranges from $\Delta y_1 = 1.65 \times 10^{-5}$ at the first point to the walls to $\Delta y_c = 6.16 \times 10^{-3}$ at the center of the channel. The value of Δy_1 corresponds to $\Delta y_1^+ = 1.65 \times 10^{-2}$ when scaled by the viscous length scale $\delta_\nu = \nu/u_\tau = 1.0 \times 10^{-3}$, where $u_\tau = \sqrt{\tau_w/\rho_f}$ is the wall-friction velocity and τ_w is the wall shear stress. The friction Reynolds number is $\mathrm{Re}_\tau = u_\tau h/\nu \approx 1000$ and the bulk Reynolds number, derived from the bulk flow velocity U_b, is $\mathrm{Re}_b = 2hU_b/\nu \approx 4 \times 10^4$.

As shown in Fig. 1, the computation is initialized with 10 000 particles that are randomly seeded in the outer layer region of the channel flow. Increasing the particle number does not change the statistical results (see Fig. 12 in the Appendix). The particles are smaller than the Kolmogorov scale and the motion of each particle is tracked through the one-way point-particle Lagrange method. The particles are driven by the Stokes drag force and a uniform external force ($\boldsymbol{F}_{\mathrm{ext}}$), pointing to the bottom wall ($y = 0$) in the wall-normal (y) direction. The governing equation for the particle motion is given by [44]

$$\frac{d\boldsymbol{x}_i}{dt} = \boldsymbol{u}_{p,i}, \tag{2a}$$

$$m_p \frac{d\boldsymbol{u}_{p,i}}{dt} = -3\pi \mu d_p (\boldsymbol{u}_{p,i} - \boldsymbol{u}_{f,i}) + \boldsymbol{F}_{\mathrm{ext}}, \tag{2b}$$

where $\boldsymbol{x}_i$ and $\boldsymbol{u}_{p,i}$ denote the position and velocity of particle i; $\boldsymbol{u}_{f,i}$ is the fluid velocity at the position of particle i, which is obtained from the online database; and m_p is the particle mass. The second term on the right-hand side of Eq. (2b), $\boldsymbol{F}_{\mathrm{ext}}$, can be regarded as a representation of any wall-normal external force, such as the effective gravitational force $\boldsymbol{F}_g = (1 - \rho_f/\rho_p)m_p \boldsymbol{g}$ in horizontal channel flows and the electrophoretic force $\boldsymbol{F}_e = \boldsymbol{E}q$ in electrostatic precipitators (ESPs) (with E being the strength of the electrostatic field and q the charge on particles). To make the results of the current work more generalizable, $\boldsymbol{F}_{\mathrm{ext}}$ is not limited to any specific force above. In each simulation run, the magnitude and the direction of $\boldsymbol{F}_{\mathrm{ext}}$ are fixed. Different values are then assigned to $|\boldsymbol{F}_{\mathrm{ext}}|$ to investigate the effect of external force magnitude. The simulation setup well reflects the situations of the gravity-induced deposition of particles in a horizontal channel and the migration of charged particles in an ESP.

The velocity in Eq. (2) is normalized by the mean bulk channel velocity $U_0 = \langle U_b \rangle = 3.1$ m/s, the length is scaled by half of the channel height $L_0 = h = 0.096$ m, and the time is scaled by the typical value $T_0 = L_0/U_0 = 0.031$ s. The particle diameter is fixed at $d_p = 4.0 \times 10^{-5}$ m and the typical mass is given by $M_0 = \rho_f L_0^3$. Other relevant parameters are the fluid density $\rho_f = 1.2$ kg/m^3, particle density $\rho_p = 0.3 \times 10^3 - 12.5 \times 10^3$ kg/m^3, and fluid kinematic viscosity $\nu = 1.5 \times 10^{-5}$ m^2/s. The simulation parameters are summarized in Table I in both dimensional and dimensionless forms. The fluid-to-particle density ratio ($\chi = \rho_f/\rho_p$) satisfies $\chi \ll 1$ and the particle volume fraction ϕ is smaller than 10^{-6}. Therefore, the added mass effect and the turbulent modulation due to particles are negligible in this work. The dimensionless form of Eq. (2b) is expressed as

$$\frac{d\hat{\boldsymbol{u}}_p}{d\hat{t}} = -\frac{\hat{\boldsymbol{v}}_s}{\mathrm{St}} - \hat{\psi}\boldsymbol{e}_y. \tag{3}$$

Here, $\hat{\boldsymbol{v}}_s = \hat{\boldsymbol{u}}_p - \hat{\boldsymbol{u}}_f$ is the dimensionless slip velocity and $\mathrm{St} = \tau_p/T_0$ stands for the Stokes number, where $\tau_p = \rho_p d_p^2/18\mu$ is the particle response time. The dimensionless external force $\hat{\psi}$ is

TABLE I. Physical and dimensionless value of the parameters in the simulation.

Parameters	Physical value	Dimensionless value
Typical scales		
Length, L_0	9.6×10^{-2} m	1
Velocity, U_0	$3.1 \, \text{ms}^{-1}$	1
Time, T_0	3.1×10^{-2} s	1
Mass, M_0	1.06×10^{-3} kg	1
Fluid properties		
Fluid density, ρ_f	$1.2 \, \text{kg m}^{-3}$	1
Fluid kinematic viscosity, υ	$1.5 \times 10^{-5} \, \text{m}^2 \, \text{s}^{-1}$	5.0×10^{-5}
Friction velocity, u_τ	$0.155 \, \text{m s}^{-1}$	5.0×10^{-2}
Viscous length, δ_υ	9.6×10^{-5} m	10^{-3}
Channel height, h	9.6×10^{-2} m	1
Bulk velocity, U_b	$3.1 \, \text{m s}^{-1}$	1
Friction velocity Reynolds number, Re_τ	–	1000
Particle properties		
Particle density, ρ_p	$0.3 \times 10^3 - 12.5 \times 10^3 \, \text{kg m}^{-3}$	$0.25 \times 10^3 - 10.4 \times 10^3$
Particle diameter, d_p	$40 \, \mu\text{m}$	4.17×10^{-4}
Particle number, N	10^4	–
Volume fraction, ϕ	8×10^{-10}	–
Viscous Stokes number, St	–	$0.01 - 1.5$
Wall-normal external force, ψ	–	$0 - 5.0$

given by

$$\hat{\psi} = \frac{6 F_{\text{ext}} L_0}{\pi \rho_p U_0^2 d_p^3}. \tag{4}$$

Hereinafter, all the variables appear in their dimensionless form and, for simplicity, the same notations as the dimensional variables are adopted. The current work focuses on the wall-normal transport of particles driven by a uniform external force. The coupling effect of particle inertia, strength of the external field, and turbulent flow is discussed within the parameter ranges St $= 0.01 - 1.5$ and $\psi = 0 - 5.0$. Within this range of Stokes number, the particle response time is much larger than the time step $\delta t = 0.0065$, ensuring the numerical accuracy. The value $\psi = 0.1$ corresponds to the situation where particles are driven by gravity (i.e., $F_{\text{ext}} = m_p g$). For charged microparticles in an electrostatic field, the electrophoretic force could be much stronger than gravity [23], which gives rise to higher values of ψ.

To validate the simulation method, we perform a simulation without external forces adopting an elastic wall condition. As shown in Fig. 2(a), the particles in the viscous sublayer exhibit a nonuniform distribution in streaks, which matches the observation of Bernardini et al. [38]. We divide the near-wall regions ($y^+ < 10$, the same value as in Marchioli and Soldati [12]) into ten equal slabs and calculate the streamwise fluid fluctuation u'_x, defined as the velocity difference between the fluid velocity seen by particles and the average fluid velocity $u_{fx} - \langle u_{fx} \rangle$ in each slab. The probability density function (PDF) of the fluid fluctuation u'_x for particles in all ten slabs is plotted in Fig. 2(b). The negative peak of the PDF indicates that particles tend to preferentially distribute in locations with lower-than-mean fluid velocities. Lighter particles (St $= 0.1$) are more likely to distribute in low-speed streaks. These characteristics are in qualitative agreement with DNS results from Marchioli and Soldati [12]. The streamwise fluid fluctuation has a wider distribution due to the fact that the turbulent flow in our simulation ($\text{Re}_\tau = 1000$) is much more intense than that in Marchioli and Soldati ($\text{Re}_\tau = 150$) [12].
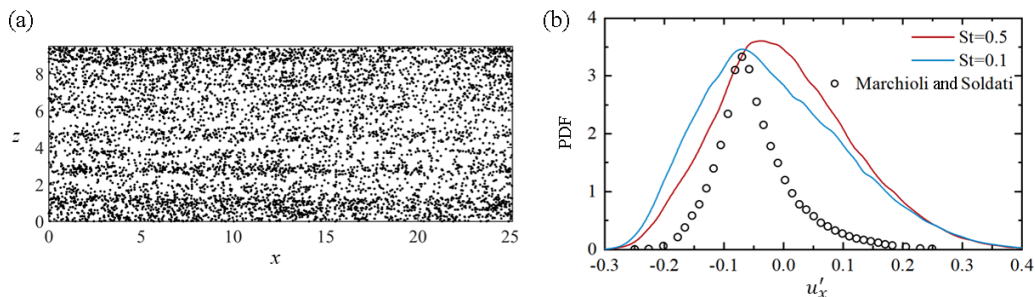
FIG. 2. (a) Instantaneous snapshot of particles with St = 0.5 in the viscous sublayer ($y^+ < 5$). (b) Probability density functions of the streamwise fluid fluctuation, $u_{fx} - \langle u_{fx} \rangle$, for St = 0.1 (blue line) and St = 0.5 (red line) in the wall region ($y^+ < 10$). The circles are the streamwise fluid fluctuations for particles with St = 0.36 from the DNS results of Marchioli and Soldati [12].

III. RESULTS AND DISCUSSION

A. Particle deposition velocity

The probability density function of the slip velocity v_s in the outer layer ($y^+ > 50$) and the deposition velocity v_d at the wall for different St and ψ values are displayed in the logarithmic coordinates in Fig. 3. As shown in Fig. 3(a), when ψ increases from 0.1 to 1, the shape of the distribution of v_s does not obviously change and the standard deviation slightly increases. The nonzero slip velocities and standard deviations indicate that small particles with Stokes number St $\ll 1.0$ deviate from the flow field in the presence of the external force field, which implies that small particles are not always faithful tracers for flow visualization and measurement [8]. From Fig. 3(b), one can see that the particle inertia (St) has a stronger impact on the PDF of v_s than the wall-normal driven force. As St increases, particles are more likely to move independently of
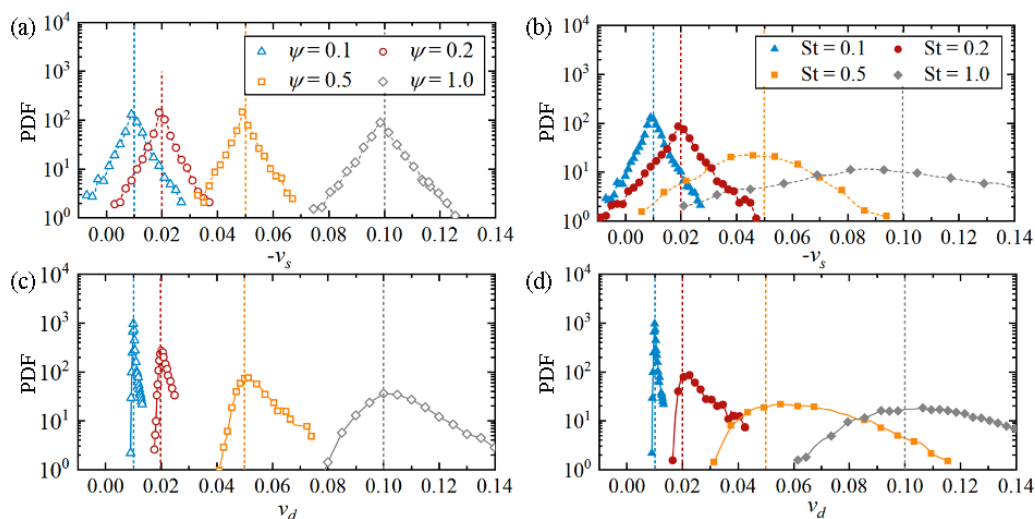

FIG. 3. (a) Probability density function (PDF) of the slip velocity v_s in the outer layer with St = 0.1 and $\psi = 0.1$ (triangles), 0.2 (circles), 0.5 (squares), and 1.0 (diamonds). (b) PDF of v_s at $\psi = 0.1$ and St = 0.1 (filled triangles), 0.2 (filled circles), 0.5 (filled squares), and 1.0 (filled diamonds). (c), (d) PDF of deposition velocity v_d for the cases with the same St and ψ as those in (a), (b), respectively. The vertical dashed lines mark the values of Stψ.
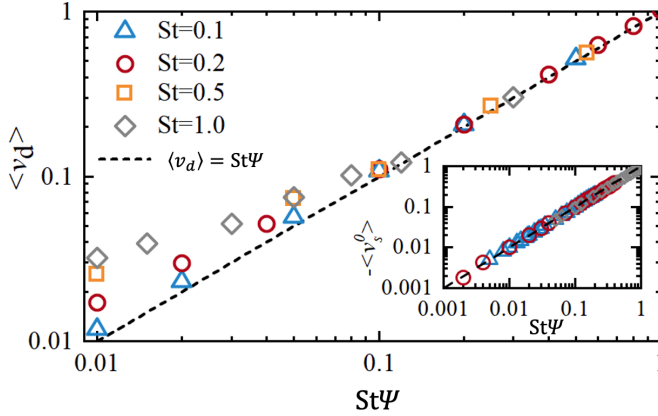
FIG. 4. Average deposition velocity $\langle v_d \rangle$ as a function of $\mathrm{St}\psi$ for particles with different Stokes numbers: St = 0.1 (triangles), 0.2 (circles), 0.5 (squares), and 1.0 (diamonds). The dashed line indicates $\langle v_d \rangle = \mathrm{St}\psi$. Inset: Average slip velocity $\langle v_s \rangle$ of particles in the outer layer ($y^+ > 50$) as a function of $\mathrm{St}\psi$ is shown in the panel.

the fluid and thus have a larger v_s. The probability distribution function of the slip velocity almost distributes symmetrically around the value $-\mathrm{St}\psi$ with all combinations of St and ψ. The correlation can be obtained by simply taking the ensemble average of Eq. (3) and assuming $\langle du_p/dt \rangle$ to be zero. The assumption $\langle du_p/dt \rangle = 0$ is reasonable at the equilibrium state in the outer layer where the turbulence is quasihomogeneous [37]. It then gives $\langle v_s^0 \rangle = -\mathrm{St}\psi$, where $\langle v_s^0 \rangle$ denotes the average slip velocity of particles in the statistically steady state (see Fig. 13 in the Appendix).

The statistics of the deposition velocity v_d are shown in Figs. 3(c) and 3(d). When the Stokes number St is fixed at 0.1 and the value of ψ is changed from 0.1 to 1, the mean value of v_d is still around $\mathrm{St}\psi$. This can be expected since the deposition velocity at the wall is equal to slip velocity since the fluid velocity is zero. However, when St is within the range $0.2-0.5$ at $\psi = 0.1$, the mean deposition velocity evidently exceeds the value of $\mathrm{St}\psi$ [see Fig. 3(d)], implying that the deposition velocity is enhanced at certain combinations of St and ψ.

The average deposition velocity $\langle v_d \rangle$ is then compared with the predicted value of $\mathrm{St}\psi$ in Fig. 4, and the average slip velocity $\langle v_s \rangle$ of particles in the outer layer ($y^+ > 50$) as a function of $\mathrm{St}\psi$ is shown in the inset of Fig. 4. It can be observed that all the data points nicely collapse onto the curve of $\langle v_s^0 \rangle = -\mathrm{St}\psi$, indicating that the average wall-normal slip velocity in the outer layer can be well predicted once the values of St and ψ are known. For a large value of $\mathrm{St}\psi$, the average deposition velocities also perfectly collapse on the line $\langle v_d \rangle = \mathrm{St}\psi$. However, for $\mathrm{St}\psi < 0.1$, an obvious deviation between $\langle v_d \rangle$ and $\mathrm{St}\psi$ appears for particles with a finite inertia (i.e., St $\geqslant 0.2$). We calculate the relative increase of the deposition velocity v_d as compared to $\mathrm{St}\psi$ to quantitatively measure the acceleration phenomenon affected by St and ψ. The relative increment of v_d is defined as

$$\Delta v_d = \frac{\langle v_d \rangle - \mathrm{St}\psi}{\mathrm{St}\psi}. \tag{5}$$

Following the previous work on the gravitational sedimentation [45], the effect of the wall-normal force ψ is grouped into a viscous scale Froude number, expressed as

$$\mathrm{Fr}^+ = \frac{u_\tau^2}{\psi \delta_v}, \tag{6}$$

where u_τ is the friction velocity and δ_v is the viscous length scale. The Froude number Fr^+ represents the ratio of the typical turbulent acceleration to the acceleration induced by the external wall-normal
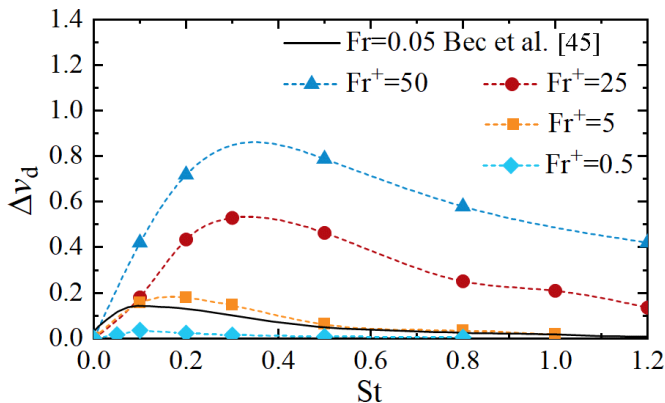
FIG. 5. Relative increment of the deposition velocity Δv_d, defined as $\langle v_d \rangle / (\mathrm{St}\psi) - 1$, as a function of Stokes number St with different viscous scale Froude numbers: $\mathrm{Fr}^+ = 50$ (triangles), 25 (circles), 5 (squares), and 0.5 (diamonds), corresponding to the external forces $\psi = 0.05, 0.1, 0.5$, and 5, respectively. The black solid line is the increment of the settling velocity due to gravity for particles in homogeneous isotropic turbulence from Bec et al. [45].

force. The relative increment of the deposition velocity Δv_d is then plotted as a function of Stokes number for different values of Fr^+ in Fig. 5. As the Stokes number increases from 0.1 to 1.2, Δv_d displays an increasing-decreasing trend, and the St dependence of Δv_d becomes weaker when Fr^+ decreases. Given a fixed value of St, a higher value of Fr^+ results in a larger Δv_d. The critical St value, where Δv_d reaches the peak value, also increases with Fr^+. Recall that a large Fr^+ value means a weak external force; the enhancement of the deposition velocity presented in Fig. 4 should be caused by the flow structures in near-wall regions. It is interesting that a similar tendency of the enhancement of particle settling velocity is observed in homogeneous isotropic turbulence [45], which is also shown in Fig. 5. The enhancement of settling velocity was attributed to the preferential sweeping of particles due to inertia bias [46], which is strongest for the largest values of Froude number [45]. In wall-bounded turbulence, the clustering of inertial particles also exits due to the vortical structures (e.g., sweeps and ejections) close to the wall [47]. The similarity between the St dependence of the deposition velocity and that of the terminal settling velocity in homogeneous isotropic turbulence (Fig. 5) indicates that the clustering of particles in near-wall vortical flow structures may cause the increase of the deposition velocity.

There are also fundamental differences between the deposition process in the wall-bounded flow and the sedimentation in homogeneous isotropic turbulence. The turbulent structures (such as counter-rotating vortices and low-speed streaks) in the near-wall region are anisotropic. In addition, the effect of the viscous sublayer, in which the turbulent effect is negligible, should be considered. It has been found that the settling velocity of particles significantly exceeded the Stokes settling velocity (characterized by $\mathrm{St}\psi$ in this work) in wall-bounded turbulent flows. This velocity enhancement was attributed to the preferential sweeping mechanism for particles at $y^+ \geqslant 100$ and to the turbophoretic effect when particles approach the wall [37]. However, it is not clear how the wall-normal external force affects this picture. In the following subsections, we analyze the transport of particles both in the region sufficiently far from the wall ($y^+ \geqslant 100$) and the region in the vicinity of the wall (the boundary layer).

B. Clustering in near-wall regions under external force

Turbulence-induced particle clustering in the near-wall regions has been extensively investigated. However, the impact of the external force on the clustering of particles is not fully understood. In this section, we investigate the particle clustering with different Stokes numbers and external force
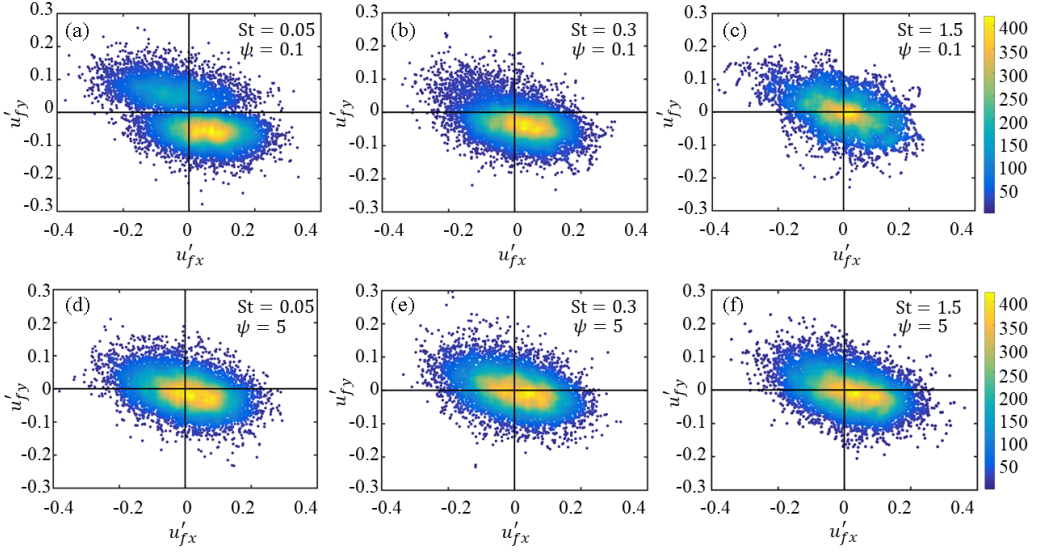
FIG. 6. Joint probability density function (indicated by the color) of the streamwise and the wall-normal fluid velocity fluctuations u'_{fx} and u'_{fy} at the particles' position when they cross the plane $y^+ = 100$ for (a), (d) St $= 0.05$, (b), (e) St $= 0.3$, and (c), (f) St $= 1.5$. The joint PDF is shown under different magnitudes of the external forces (a)–(c) $\psi = 0.1$ (Fr$^+ = 25$) and (d)–(f) $\psi = 5$ (Fr$^+ = 0.5$).

magnitudes and correlate it with the deposition velocity. The quadrant analysis is adopted to show the correlation between the particle distribution and the coherent flow motions [48]. The fluctuations of the flow velocity at the particle position are calculated as

$$u'_{fx} = u_{fx} - \langle u_{fx}\rangle, \tag{7a}$$

$$u'_{fy} = u_{fy} - \langle u_{fy}\rangle, \tag{7b}$$

where $\langle u_{f,x/y}\rangle$ is the average fluid velocity and the subscripts x and y denote the streamwise and wall-normal directions (with positive direction pointing away from the wall), respectively. In the $u'_{fx} - u'_{fy}$ plane, four kinds of events can be identified [49]: first quadrant events Q1 ($u'_{fx} > 0$, $u'_{fy} > 0$) with outward motion of high-speed fluid; second quadrant events Q2 ($u'_{fx} < 0$, $u'_{fy} > 0$) with outward motion of low-speed fluid, which is also known as the low-speed streak lifting; third quadrant events Q3 ($u'_{fx} < 0$, $u'_{fy} < 0$) with inward motion of low-speed fluid; fourth quadrant events Q4 ($u'_{fx} > 0$, $u'_{fy} < 0$) with inward motion of high-speed fluid. The second and fourth quadrant events contribute to the negative Reynolds stress and are known as ejections and sweeps. Since the particles are removed from the computational domain when they hit the wall, the velocity information is collected when particles approach the wall. The nonequilibrium information represents the transfer mechanism of particles from the flow to the wall and is different from the steady-state statistics when particles reach an equilibrium distribution [16,17].

The distribution of particles in the $u'_{fx} - u'_{fy}$ plane is shown in Figs. 6(a)–6(c) at $\psi = 0.1$ (Fr$^+ = 25$) for particles with St $= 0.05$, 0.3, and 1.5 in the layer of $y^+ = 100$. The data points are colored according to the joint probability density function of the velocity fluctuations. When St $= 0.05$, two modes of particle distribution in the $u'_{fx} - u'_{fy}$ plane are observed: Most particles are distributed in Q4, and a considerable fraction of particles is found in Q2. This indicates that the particles with small inertia can be entrained in sweeps and ejections. For particles with St $= 0.3$, the clustering of particles in Q2 vanishes and most particles are concentrated in Q4, indicating that sweeps govern the particle motions. For the case with St $= 1.5$, the peak of the joint PDF is around the origin, indicating that heavy particles do not undergo an obvious clustering in coherent structures. The
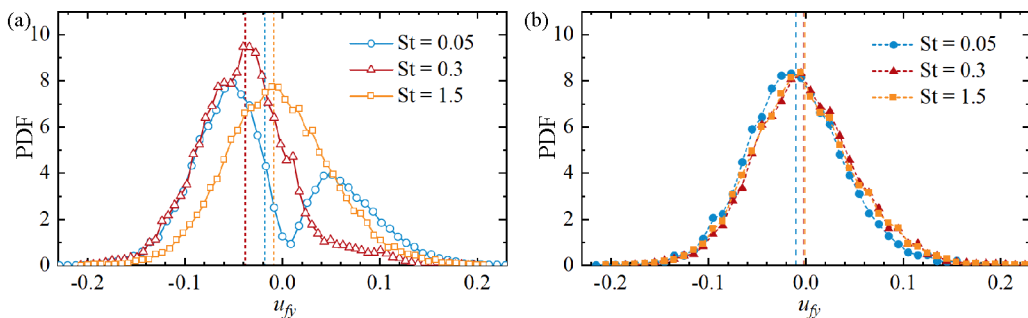
FIG. 7. Probability density function of the wall-normal flow velocity u_{fy} at the particle position at $y^+ = 100$ for different Stokes numbers with (a) a weak external force $Fr^+ = 25$ ($\psi = 0.1$) and (b) a strong external force $Fr^+ = 0.5$ ($\psi = 5$) and St = 0.05 (circles), 0.3 (triangles), and 1.5 (squares). The vertical dashed lines mark the average values $\langle u_{fy} \rangle$ for different Stokes numbers.

distribution of particles in the $u'_{fx} - u'_{fy}$ plane with a strong external force at $\psi = 5$ ($Fr^+ = 0.5$) are shown in Figs. 6(d)–6(f). Particles distribute around the origin for all Stokes numbers (St = 0.05, 0.3, and 1.5). Given such a strong external force, particles settle very fast and the clustering of particles is inhibited by the crossing trajectory effect [16,50].

The preferential distribution due to particle inertia leads to a significant difference in the wall-normal flow velocity at the particle position. The probability density functions of the wall-normal velocity at the particle position (termed as u_{fy}) at $y^+ = 100$ for different Stokes numbers are shown in Fig. 7(a) at $Fr^+ = 25$ (corresponding to $\psi = 0.1$). Two peaks, one at positive u_{fy} and one at negative u_{fy}, appear on the curve at St = 0.05. When St = 0.3, there is only one peak at a negative value of u_{fy}. As St further increases to 1.5, the peak of the PDF curve moves back to the origin. The magnitude of the average wall-normal flow velocity at the particle position, represented by the vertical dashed line, first increases and then decreases with St. The PDFs of the wall-normal fluid velocity sampled by particles under the strong external force at $Fr^+ = 0.5$ ($\psi = 5$) are shown in Fig. 7(b). The PDF curves for all Stokes numbers almost overlap and the peaks locate around the origin, indicating that particles do not undergo the preferential distribution during the deposition process (known as the crossing trajectory effect). The suppression of the preferential distribution under strong external forces is in accordance with the observation at $Fr^+ = 0.5$ and 5 in Fig. 5, where the magnitude of $\langle v_d \rangle / (St\psi) - 1$ decreases and its dependence on St becomes weak as ψ increases.

C. Particle dynamics in boundary layer

The statistical results in the previous subsection are collected at a fixed wall-normal distance ($y^+ = 100$) and show that the clustering of inertia particles is strongly affected by the external forces. To understand how the combined effect of the clustering and external forces impacts the particle deposition velocity, one needs to know how the statistics vary with the particle-to-wall distance. In the viscous sublayer, the flow velocity and its fluctuation undergo an abrupt decrease and particles are markedly decelerated in the viscous sublayer. Only particles with a sufficiently large wall-normal velocity before entering the viscous sublayer and large inertia can impact the wall (such as particles with the free-flight mechanism). In the absence of the external force, these particles are only of a limited portion [32,33]. Applying a wall-normal external force results in an enhanced deposition fraction.

The conditional probability density functions of the wall-normal fluid velocity at particle position u_{fy} and the particle velocity u_{py} are calculated at different wall-normal distances y^+ for St = 0.05, 0.3, and 1.5. As shown in Fig. 8, for all three Stokes numbers, the PDF of u_{fy} does not significantly change when the particle-to-wall distance y^+ varies from 200 to 50. However, as particles move
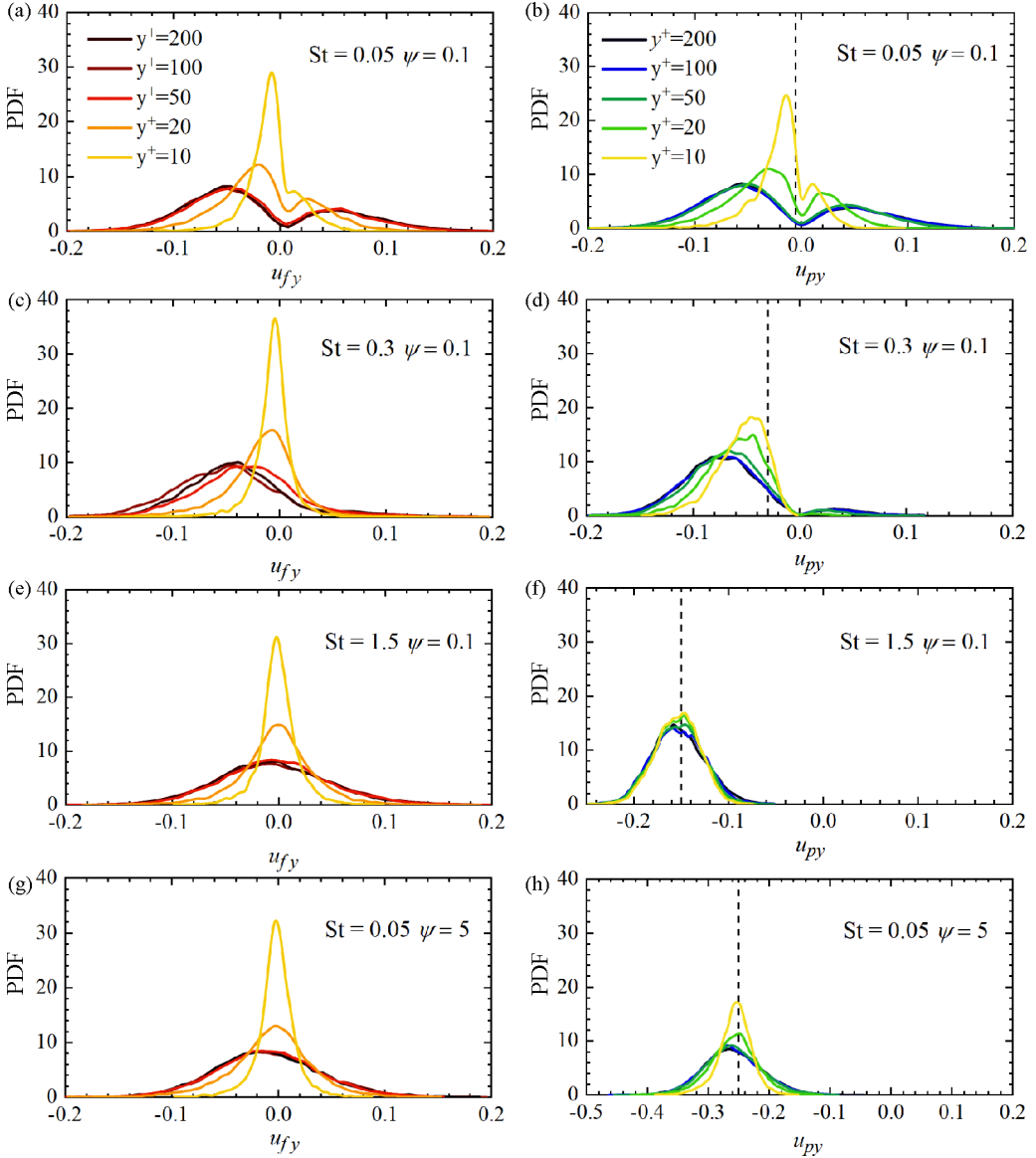
FIG. 8. Conditional probability density function of the wall-normal flow velocity u_{fy} at the particle position (a), (c), (e), (g) and the conditional PDF of the wall-normal particle velocity u_{py} (b), (d), (f), (h) for (a), (b) St $= 0.05$, (c), (d) St $= 0.3$, and (e), (f) St $= 1.5$ at $\psi = 0.1$ (Fr$^+ = 25$). (g), (h) are results for St $= 0.05$ and $\psi = 5$ (i.e., strong external force, Fr$^+ = 0.5$).

into the buffer layer and the viscous sublayer ($y^+ < 30$), the flow velocity in all cases tends to distribute around zero because of the vanishing of the flow velocity. A considerable discrepancy can be observed in particle velocity distributions for different Stokes numbers. For St $= 0.05$ [Figs. 8(a) and 8(b)], the shape of the PDF curves of u_{py} is essentially the same as those for u_{fy} and the mean value of the difference between u_{py} and u_{fy}, $\langle u_{py} - u_{fy} \rangle$, is close to St$\psi$. The particles with such small inertia can quickly respond to the variation of underlying flow velocity; the enhancement of the deposition velocity thus is negligible. With a large inertia (St $= 1.5$), the particle velocity
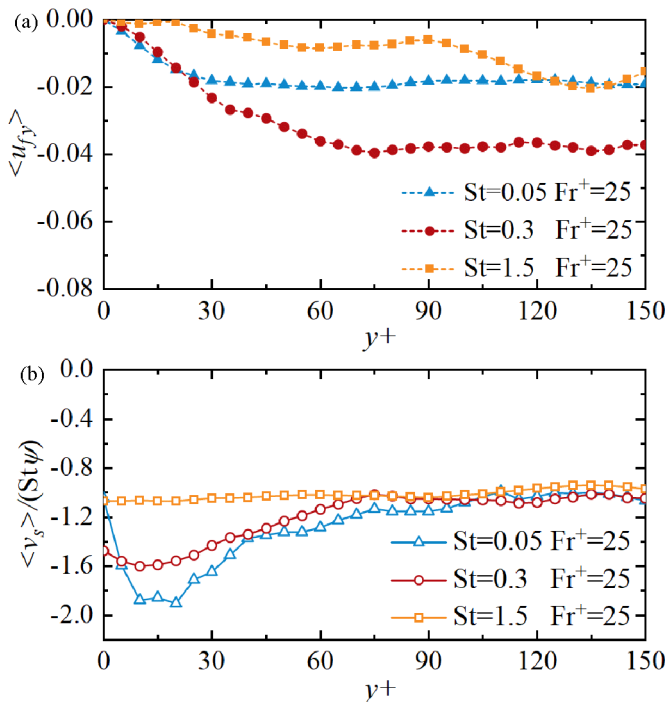
FIG. 9. (a) Mean value of the wall-normal fluid velocity $\langle u_{fy} \rangle$ at the particle position as a function of the wall-normal distance y^+ with different Stokes numbers: St = 0.05 (triangles), 0.3 (circles), and 1.5 (squares). (b) Mean slip velocity $\langle v_s \rangle$, scaled by the predicted value Stψ, as a function of y^+. The viscous scale Froude number Fr$^+$ is fixed at 25, corresponding to $\psi = 0.1$.

is almost independent of the local flow field [see Figs. 8(e) and 8(f)]. The deposition velocity is dominated by the external driven force, which yields $v_d \approx$ Stψ. Given a moderate inertia (St = 0.3), the particles obtain a large momentum due to the preferential concentration in the high-velocity near-wall regions. As a result of the finite particle inertia, the particles' wall-normal velocity cannot be fully reduced by the fluid inside the buffer layer and the viscous sublayer, leading to a high deposition velocity. It explains why the enhancement of the deposition velocity (i.e. $v_d >$ Stψ) is most significant for particles with a moderate Stokes number.

In Figs. 8(g) and 8(h), the PDFs of u_{py} and u_{fy} for particles with small inertia (St = 0.05) but a strong external force (Fr$^+$ = 0.5) are displayed. The correlation between u_{py} and u_{fy} is obviously reduced. The fluid velocity seen by particles distributes around the origin, which is similar to the large inertia cases in Fig. 8(e). The mean particle velocity during the deposition process thus is close to Stψ.

The average wall-normal flow velocity at particle locations $\langle u_{fy} \rangle$ and the average particle slip velocity $\langle v_s \rangle$ (scaled by Stψ) are plotted as a function of the particle-to-wall distance y^+ for St = 0.05, 0.3, and 1.5 in Fig. 9. Outside the buffer layer, the magnitude of the average flow velocity $|\langle v_s \rangle|$ for St = 0.3 is the largest due to the preferential distribution. When particles enter the buffer layer ($y^+ <30$), the sudden decrease of the fluid velocity causes the increase of the wall-normal slip velocity for small and moderate Stokes numbers in Fig. 9(b). Particles with St = 0.05 then quickly decelerate to $|\langle v_s \rangle| \approx$ Stψ in the viscous sublayer, while for particles with a moderate inertia St = 0.3, the thickness of the viscous sublayer is not sufficiently large for the relaxation of particle velocity and hence the slip velocity only slightly decreases from 1.6Stψ to 1.5Stψ before colliding with the wall. Heavy particles (St = 1.5) undergo a ballistic motion and the average slip velocity

stays at $|\langle v_s \rangle| \approx \mathrm{St}\psi$ over the entire near-wall region until the particles collide with the wall. For heavy particles, the migration velocity ($\mathrm{St}\psi = 0.1$) due to the external force is much larger than the flow velocity at particle positions; the fluctuation of $\langle u_{fy} \rangle$ in Fig. 9(a) does not obviously affect the curve of the scaled slip velocity $\langle v_s \rangle / (\mathrm{St}\psi)$.

Summarizing the results above, we identify two factors that lead to the enhancement of the deposition velocity for particles with moderate inertia: (a) the preferential distribution of particles in the near-wall high-velocity regions (Fig. 6) and (b) the insufficient deceleration of particles in the viscous sublayer [Fig. 8(b)].

To quantitatively measure the combined effect of particle inertia (St), external force (ψ), and the deceleration in the viscous sublayer, one can compare the relaxion distance L_R (dimensionless) with the dimensionless thickness of the viscous sublayer Y_0. The deceleration of particles in the viscous sublayer is approximated as a settling process driven by an external force in a stationary flow. Such an approximation is reasonable when the particle inertia is large or the external force is strong (i.e., free-flight particles), for which the influence of the small flow fluctuation in the viscous sublayer can be neglected. In the still flow field, the evolution of the particle velocity with initial settling velocity u_{p0} and the terminal settling velocity $\mathrm{St}\psi$ follows

$$\frac{u_p(t) - \mathrm{St}\psi}{u_{p0} - \mathrm{St}\psi} = \exp\left(-\frac{t}{\mathrm{St}}\right). \tag{8}$$

Integrating $u_p(t)$ in Eq. (8) from $t = 0$ to $t = \mathrm{St}$ (dimensionless relaxation time), the relaxation length of the particle L_R can be obtained as

$$L_R = \mathrm{St}(u_{p0} - \mathrm{St}\psi)\left(1 - \frac{1}{e}\right) + \mathrm{St}^2\psi. \tag{9}$$

We then take $y_0^+ = 5$ (viscous sublayer) as the starting point of the particle deceleration process, which gives

$$Y_0 = y_0^+ \upsilon \sqrt{\frac{\rho}{\tau_w}}. \tag{10}$$

If the free-flight model is valid, from (9) and (10), the deposition velocity v_d, the particle velocity at the starting point u_{p0}, and the deposition time t_d follows:

$$\frac{v_d - \mathrm{St}\psi}{u_{p0} - \mathrm{St}\psi} = \exp\left(-\frac{t_d}{\mathrm{St}}\right) \equiv \chi, \tag{11}$$

$$Y_0 = \mathrm{St}(u_{p0} - \mathrm{St}\psi)\left[1 - \exp\left(-\frac{t_d}{\mathrm{St}}\right)\right] + \mathrm{St}\psi t_d, \tag{12}$$

Eliminating t_d in (11) and (12), we obtain

$$Y_0 = \mathrm{St}(u_{p0} - \mathrm{St}\psi)(1 - \chi) - \mathrm{St}^2\psi \ln \chi. \tag{13}$$

In Fig. 10, the dimensionless velocity χ is plotted as a function of Y_0/L_R for particles with three different Stokes numbers St = 0.05, 0.3, and 1.5 and varying ψ. To avoid the error caused by a near-zero denominator when u_{p0} is close to $\mathrm{St}\psi$, we choose the particles with $1.2\mathrm{St}\psi < u_{p0} < 3\mathrm{St}\psi$. The data points in Fig. 10 are DNS results of χ for each particle and the dashed and solid lines stand for the solutions of Eq. (13) when $u_{p0} = 1.2\mathrm{St}\psi$ and $3\mathrm{St}\psi$, respectively. The simulation results distribute around the solutions of Eq. (13). This suggests that there is a similarity between the deceleration of particles in the viscous sublayer and the settling process in a stationary flow. Particles with a larger Stokes number tend to have a larger value of χ, which stands for an insufficient deceleration. When $Y_0/L_R \gg 1$, the particle deposition velocity is close to the terminal velocity ($\mathrm{St}\psi$). In contrast, when $Y_0/L_R < 1$, the deposition velocity is determined by the flow transport and the external force outside the boundary layer. Equation (13) can reflect the combined effect of particle inertia (St), the external force (ψ), and the thickness of the viscous sublayer (Y_0). The
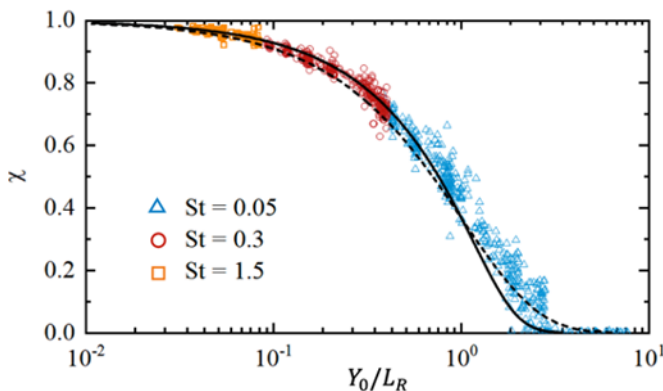
FIG. 10. Ratio of the velocity difference between the particle velocity and the Stokes settling velocity at $y^+ = 0$ and $y^+ = 5$, $\chi = (v_d - \text{St}\psi)/(u_{p0} - \text{St}\psi)$, versus Y_0/L_R, where Y_0 is the thickness of the viscous sublayer and L_R is the relaxation distance of particles. The solid and dashed lines mark the theoretical solutions of Eq. (13) when $u_{p0} = 1.2\text{St}\psi$ (dashed line) and $u_{p0} = 3\text{St}\psi$ (solid line), respectively.

clustering of particles in the coherent flow structures affects the velocity u_{p0} of particles when they enter the viscous sublayer; therefore, the effect of clustering is also included in Eq. (13).

The deposition mechanisms of particles with different inertia and a wall-normal external force are summarized in Fig. 11. The deposition velocity depends on two aspects: (1) the entrainment of particles in the flow coherent structures in the near-wall regions; (2) the deceleration of particles in the boundary layer. We found these two effects strongly depend on particle inertia (St) and the intensity of the wall-normal external force (ψ). With a weak external force, some of the light particles (St = 0.05) are transferred toward the wall in sweep events (Q2) and then reentrained back in ejection events (Q4), and the others deposit on the wall after a considerable deceleration process; particles with moderate inertia (St = 0.3) are entrained by sweeps toward the wall and undergo an insufficient deceleration process; no obvious clustering is observed for heavy particles (St = 1.5), and particles barely decelerate in the boundary layer. Given a strong force, the clustering of particles is inhibited due to the effect of the crossing trajectory; the deposition velocity of particles is determined by the external driven force, which yields $v_d = \text{St}\psi$. Consequently, the deposition
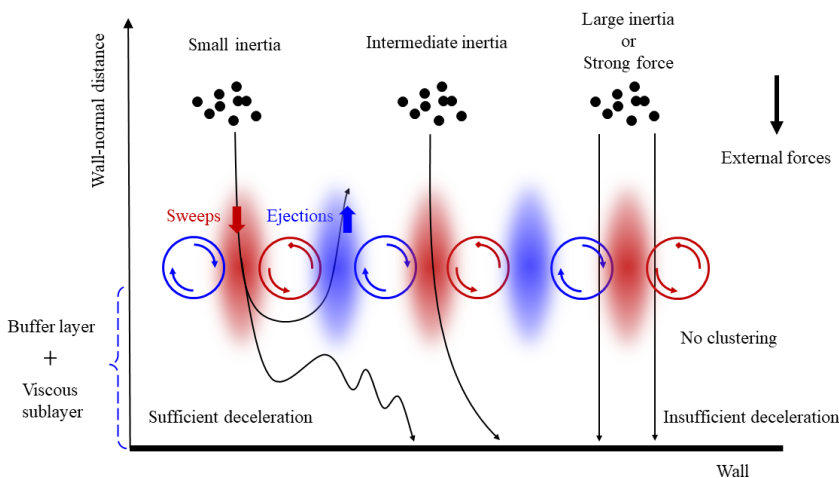

FIG. 11. Mechanisms of the deposition of particles with different inertia and external force magnitudes.

velocity of particles with moderate inertia under a weak external force is significantly enhanced compared with the Stokes settling velocity $St\psi$.

Indeed, it has been previously reported that the external force can enhance the settling velocity of particles due to the preferential sweeping and the turbophoretic drift in the boundary layer [37]. However, this phenomenon is only considered for different particle inertia with a fixed value of the driving force. In the current work, we demonstrate that increasing the external driving force suppresses the preferential distribution of particles and, hence, inhibits the enhancement of the deposition velocity $[\langle v_d \rangle / (St\psi) - 1]$. This is the key difference between our study and the previous work.

IV. CONCLUSIONS

In summary, the migration and deposition of particles in a turbulent channel flow with a wall-normal force is investigated using the DNS and point-particle simulations. The main purpose of the current work is to investigate the influence of the external force on the deposition velocity of particles. The average deposition velocity $\langle v_d \rangle$ can be significantly larger than the Stokes settling velocity $St\psi$ at certain values of particle inertia (St) and the external force magnitudes (ψ). The increment of the deposition velocity, $\langle v_d \rangle / (St\psi) - 1$, shows an increasing-decreasing trend as the Stokes number St increases and is most significant for particles with moderate inertia. The enhancement of the deposition velocity, however, is inhibited when the external force is sufficiently strong. Given a weak force ($\psi = 0.1$), particles with small inertia (St = 0.05) are entrained in sweeps and ejections, whereas particles with St = 0.3 are concentrated in sweeps. Heavy particles (St = 1.5) do not undergo an obvious clustering in coherent structures. These findings resemble the results in previous studies [15–17,19]. The inhibition of the preferential distribution by the external force is demonstrated through the quadrant analysis, based on the fluctuation of the flow velocity at the particle position. Given a strong external force ($\psi = 5$), particles distribute around the origin in the $u'_{fx} - u'_{fy}$ plane for all Stokes numbers, indicating that the clustering of particles is suppressed.

The PDFs of the wall-normal particle velocity and flow velocity at particle positions are then measured at different y^+ values. According to the evolution of the two PDFs as y^+ decreases, we identify the second factor that affects the deposition velocity, i.e., the insufficient deceleration of inertial particles in the viscous sublayer. The particles with moderate inertia (St = 0.3) obtain large momentum due to the preferential concentration in the high-velocity near-wall regions and, as a result of the finite particle inertia, the velocity cannot be fully reduced by the low-velocity fluid inside the viscous sublayer, leading to an obvious enhancement of the deposition velocity. Changing the external force results in a variation in the velocity of the particles when they enter the viscous sublayer and in the relaxation distance. The combined effect of particle inertia, the external force, and the flow structure on the particle deposition velocity can be well described by the parameter, Y_0/L_R, which is the ratio between the thickness of viscous sublayer Y_0 and the particle relaxation distance L_R. When $Y_0/L_R \gg 1$, the particle deposition velocity is close to the terminal velocity ($St\psi$). In contrast, when $Y_0/L_R < 1$, the deposition velocity is determined by the flow transport and the external force outside the boundary layer.

There are several interesting directions for future research. In the current work, the one-way coupled method is adopted, in which the particle-particle and particle-turbulence interactions are ignored. In the near-wall region, the clustering of particles can lead to an increase of local particle concentration; as a result, the interactions between particles [51–53] and the modulation of the flow by particles [54,55] may have a non-negligible effect. Moreover, most of the previous studies focused on one-point statistics of particles. Further effort can be dedicated to understanding particle pair dynamics, which is essential to modeling the collision kernel.
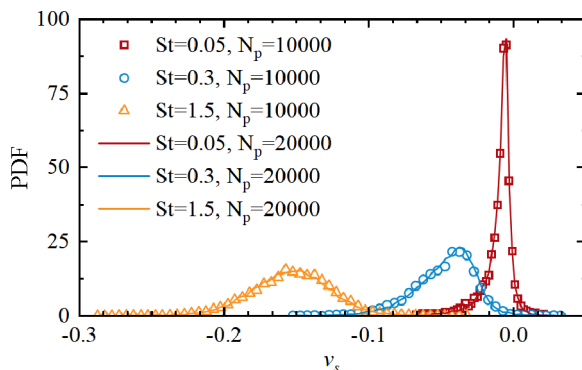
ACKNOWLEDGMENTS

FIG. 12. Probability density function of the slip velocity in the buffer layer $y^+ = 10$ for particles with Stokes number St = 0.05, 0.3, and 1.5, with particle number $N_p = 10\,000$ (symbols) and 20 000 (lines), respectively.

APPENDIX: PARTICLE NUMBER INDEPENDENCE AND STATISTICAL STEADY STATE

The probability density functions of the slip velocity in the buffer layer ($y^+ = 10$) for different particle numbers are shown in Fig. 12. It can be observed that increasing the particle number does not affect the velocity distribution, indicating the particle number in this work ($N_p = 10\,000$) is large enough to ensure reasonable statistics.
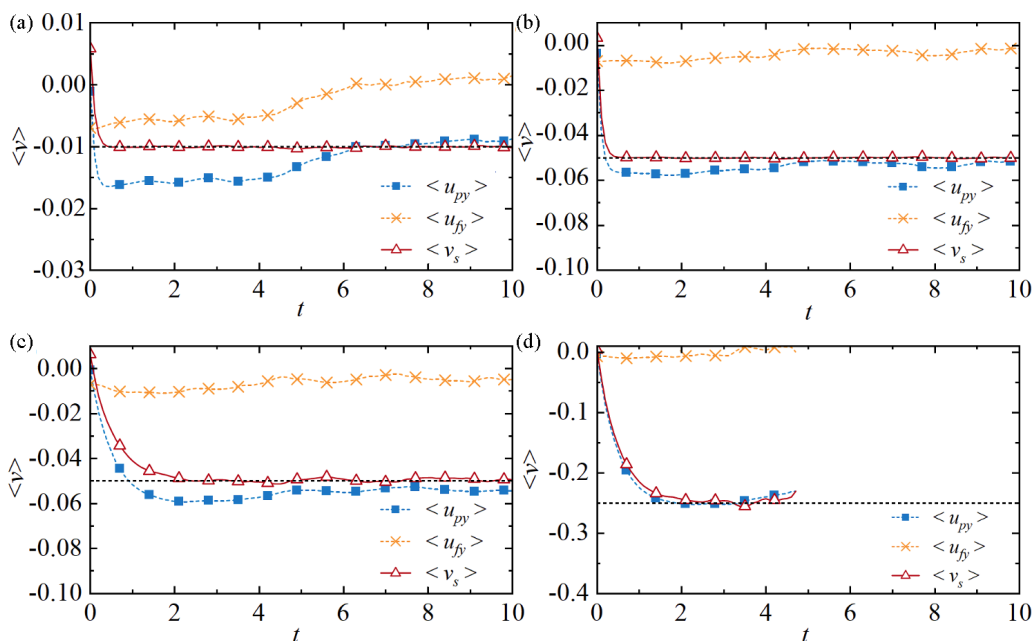

FIG. 13. Temporal evolution of the mean particle wall-normal velocity $\langle u_{py} \rangle$ (solid squares), mean wall-normal fluid velocity at the center of particles $\langle u_{fy} \rangle$ (crosses), and mean wall-normal slip velocity $\langle v_s \rangle$ (open triangles). The values are averaged over all particles in the outer layer region of the channel flow. Four cases are shown with (a) St = 0.1, $\psi = 0.1$, (b) St = 0.1, $\psi = 0.5$, (c) St = 0.5, $\psi = 0.1$, and (d) St = 0.5, $\psi = 0.5$. The horizontal dashed line in each panel marks the value of $-\text{St}\psi$.

Since our particles are seeded randomly in the outer layer with zero velocity, particles will experience an acceleration process under the effect of wall-normal forces. The evolution of the mean wall-normal particle velocity $\langle u_{py} \rangle$, the mean wall-normal flow velocity $\langle u_{fy} \rangle$ at the center of the particles, and the mean wall-normal slip velocity $\langle v_s \rangle = \langle u_{py} - u_{fy} \rangle$ is presented in Fig. 13 (with positive direction pointing away from the wall). The magnitude of the slip velocity $\langle v_s \rangle$ undergoes a fast increase at the initial stage and then enters a plateau, in which $\langle v_s \rangle$ remains almost constant at the equilibrium state. Since particles are removed upon colliding on the wall, the simulation time will be shorter for the cases with a large value of St or ψ [see Fig. 13(d)]. However, the statistical results in this work come from the equilibrium state.

---

[1] J. C. Salevan, A. H. Clark, M. D. Shattuck, C. S. O'Hern, and N. T. Ouellette, Determining the onset of hydrodynamic erosion in turbulent flow, Phys. Rev. Fluids **2**, 114302 (2017).

[2] T. Pähtz, A. H. Clark, M. Valyrakis, and O. Durán, The physics of sediment transport initiation cessation and entrainment across aeolian and fluvial environments, Rev. Geophys. **58**, e2019RG000679 (2020).

[3] A. Jaworek, A. Marchewicz, A. Sobczyk, A. Krupa, and T. Czech, Two-stage electrostatic precipitators for the reduction of PM2.5 particle emission, Prog. Energy Combust. Sci. **67**, 206 (2018).

[4] A. Suman, N. Casari, E. Fabbri, M. Pinelli, L. Di Mare, and F. Montomoli, Gas turbine fouling tests: Review, critical analysis, and particle impact behavior map, J. Eng. Gas Turbine Power. **141**, 3 (2019).

[5] S. T. W. Kuruneru, K. Vafai, E. Sauret, and Y. Gu, Application of porous metal foam heat exchangers and the implications of particulate fouling for energy-intensive industries, Chem. Eng. Sci. **228**, 115968 (2020).

[6] A. Guha, Transport and deposition of particles in turbulent and laminar flow, Annu. Rev. Fluid Mech. **40**, 311 (2008).

[7] M. Di Renzo, P. L. Johnson, M. Bassenne, L. Villafañe, and J. Urzay, Mitigation of turbophoresis in particle-laden wall-bounded turbulence by using incident electric fields, Phys. Rev. Fluids. **4**, 124303 (2019).

[8] V. Mathai, E. Calzavarini, J. Brons, C. Sun, and D. Lohse, Microbubbles and Microparticles Are Not Faithful Tracers of Turbulent Acceleration, Phys. Rev. Lett. **117**, 024501 (2016).

[9] M. Caporaloni, F. Tampieri, F. Trombetti, and O. Vittori, Transfer of particles in nonisotropic air turbulence, J. Atmos. Sci. **32**, 565 (1975).

[10] M. W. Reeks, The transport of discrete particles in inhomogeneous turbulence, J. Aerosol Sci. **14**, 729 (1983).

[11] G. Sardina, P. Schlatter, L. Brandt, F. Picano, and C. M. Casciola, Wall accumulation and spatial localization in particle-laden wall flows, J. Fluid Mech. **699**, 50 (2012).

[12] C. Marchioli and A. Soldati, Mechanisms for particle transfer and segregation in a turbulent boundary layer, J. Fluid Mech. **468**, 283 (2002).

[13] D. W. Rouson and J. K. Eaton, On the preferential concentration of solid particles in turbulent channel flow, J. Fluid Mech. **428**, 149 (2001).

[14] Y. Jie, Z. Cui, C. Xu, and L. Zhao, On the existence and formation of multi-scale particle streaks in turbulent channel flows, J. Fluid Mech. **935**, A18 (2022).

[15] A. D. Bragg, D. H. Richter, and G. Wang, Settling strongly modifies particle concentrations in wall-bounded turbulent flows even when the settling parameter is asymptotically small, Phys. Rev. Fluids **6**, 124301 (2021).

[16] V. Lavezzo, A. Soldati, S. Gerashchenko, Z. Warhaft, and L. R. Collins, On the role of gravity and shear on inertial particle accelerations in near-wall turbulence, J. Fluid Mech **658**, 229 (2010).

[17] M. Ebrahimian, R. S. Sanders, and S. Ghaemi, Dynamics and wall collision of inertial particles in a solid–liquid wall-bounded turbulence, J. Fluid Mech. **881**, 872 (2019).

[18] Y. Wang, K. M. Lam, and Y. Lu, Settling velocity of fine heavy particles in turbulent open channel flow, Phys. Fluids **30**, 095106 (2018).

[19] J. Lee and C. Lee, The effect of wall-normal gravity on particle-laden near-wall turbulence, J. Fluid Mech. **873**, 475 (2019).

[20] S. Lee and C. Lee, Behavior of settling particles in homogeneous shear turbulence, Phys. Rev. Fluids **5**, 104306 (2020).

[21] H. Zhu, C. Pan, G. Wang, Y. Liang, X. Ji, and J. Wang, Attached eddy-like particle clustering in a turbulent boundary layer under net sedimentation conditions, J. Fluid Mech. **920**, A53 (2021).

[22] J. B. Mclaughlin, Aerosol particle deposition in numerically simulated channel flow, Phys. Fluids. A **1**, 1211 (1989).

[23] A. Soldati, P. Andreussi, and S. Banerjee, Direct simulation of turbulent particle transport in electrostatic precipitators, AIChE J. **39**, 1910 (1993).

[24] M. Soltani and G. Ahmadi, Charged particle trajectory statistics and deposition in a wall-bounded turbulence, Aerosol Sci. Technol. **31**, 170 (1999).

[25] Y. Yao and J. Capecelatro, An accurate particle-mesh method for simulating charged particles in wall-bounded flows, Powder Technol. **387**, 239 (2021).

[26] N. Gao, J. Niu, Q. He, T. Zhu, and J. Wu, Using RANS turbulence models and Lagrangian approach to predict particle deposition in wall-bounded turbulence, Build. Environ. **48**, 206 (2012).

[27] L. Tian and G. Ahmadi, Particle deposition in turbulent duct flows—comparisons of different model predictions, J. Aerosol Sci. **38**, 377 (2007).

[28] A. C. K. Lai, M. A. Byrne, and A. J. H. Goddard, Measured deposition of aerosol particles on a two-dimensional ribbed surface in a turbulent duct flow, J. Aerosol Sci. **30**, 1201 (1999).

[29] W. Kvasnak, G. Ahmadi, R. Bayer, and M. Gaynes, Experimental investigation of dust particle deposition in a turbulent channel flow, J. Aerosol Sci. **24**, 795 (1993).

[30] T. L. Montgomery and M. Corn, Aerosol deposition in a pipe with turbulent airflow, J. Aerosol Sci. **1**, 185 (1970).

[31] S. K. Friedlander and H. F. Johnstone, Deposition of suspended particles from turbulent gas streams, Ind. Eng. Chem. **49**, 1151 (1957).

[32] C. Narayanan, D. Lakehal, L. Botto, and A. Soldati, Mechanisms of particle deposition in a fully developed turbulent open channel flow, Phys. Fluids. **15**, 763 (2003).

[33] A. Soldati and C. Marchioli, Physics and modelling of turbulent particle deposition and entrainment: Review of a systematic study, Int. J. Multiphase Flow. **35**, 827 (2009).

[34] J. W. Cleaver and B. Yates, A sub layer model for the deposition of particles from a turbulent flow, Chem. Eng. Sci. **30**, 983 (1975).

[35] B. Zhao and J. Wu, Modeling particle deposition from fully developed turbulent flow in ventilation duct, Atmos. Environ. **40**, 457 (2006).

[36] H. Lu and Y. Wang, Particle deposition in ventilation ducts: A review, Build. Simul. **12**, 723 (2019).

[37] A. D. Bragg, D. H. Richter, and G. Wang, Mechanisms governing the settling velocities and spatial distributions of inertial particles in wall-bounded turbulence, Phys. Rev. Fluids **6**, 064302 (2021).

[38] M. Bernardini, Reynolds number scaling of inertial particle statistics in wall-bounded turbulence, J. Fluid Mech. **758**, R1 (2014).

[39] P. L. Johnson, M. Bassenne, and P. Moin, Turbophoresis of small inertial particles: Theoretical considerations and application to wall-modelled large-eddy simulations, J. Fluid Mech. **883**, A27 (2020).

[40] L. Brandt and F. Coletti, Particle-laden turbulence: Progress and perspectives, Annu. Rev. Fluid Mech. **54**, 159 (2022).

[41] E. Perlman, R. Burns, Y. Li, and C. Meneveau, Data exploration of turbulence simulations using a database cluster, in *Proceedings of the 2007 ACM/IEEE Conference on Supercomputing SC07* (Association for Computing Machinery, New York, 2007).

[42] Y. Li, E. Perlman, M. Wan, Y. Yang, C. Meneveau, R. Burns, S. Chen, A. Szalay, and G. Eyink, A public turbulence database cluster and applications to study Lagrangian evolution of velocity increments in turbulence, J. Turbul. **9**, N31 (2008).

[43] J. Graham, K. Kanov, X. I. A. Yang, M. Lee, N. Malaya, C. C. Lalescu, R. Burns, G. Eyink, A. Szalay, R. D. Moser, and C. Meneveau, A web services accessible database of wall-bounded turbulence and its use for testing a new integral wall model for LES, J. Turbul. **17**, 181 (2016).

[44] M. R. Maxey and J. J. Riley, Equation of motion for a small rigid sphere in a nonuniform flow, Phys. Fluids. **26**, 883 (1983).

[45] J. Bec, H. Homann, and S. S. Ray, Gravity-Driven Enhancement of Heavy Particle Clustering in Turbulent Flow, Phys. Rev. Lett. **112**, 184501 (2014).

[46] L. P. Wang and M. R. Maxey, Settling velocity and concentration distribution of heavy particles in homogeneous isotropic turbulence, J. Fluid Mech. **256**, 27 (1993).

[47] R. J. Adrian, C. D. Meinhart, and C. D. Tomkins, Vortex organization in the outer region of the turbulent boundary layer, J. Fluid Mech. **422**, 1 (2000).

[48] J. M. Wallace, H. Eckelmann, and R. S. Brodkey, The wall region in turbulent shear flow, J. Fluid Mech. **54**, 39 (1972).

[49] S. B. Pope, *Turbulent Flows* (Cambridge University Press, Cambridge, 2000).

[50] A. J. Dorgan and E. Loth, Simulation of particles released near the wall in a turbulent boundary layer, Int. J. Multiphase Flow **30**, 649 (2004).

[51] S. Chen, S. Li, and J. S. Marshall, Exponential scaling in early-stage agglomeration of adhesive particles in turbulence, Phys. Rev. Fluids **4**, 024304 (2019).

[52] S. Chen and S. Li., Collision-induced breakage of agglomerates in homogenous isotropic turbulence laden with adhesive particles, J. Fluid Mech. **902**, A28 (2020).

[53] P. Chen, S. Chen, M. Yang, and S. Li, Falling clouds of particles with finite inertia in viscous flows, Phys. Fluids **33**, 033314 (2021).

[54] B. Yang, C. Peng, G. Wang, and L. P. Wang, A direct numerical simulation study of flow modulation and turbulent sedimentation in particle-laden downward channel flows, Phys. Fluids **33**, 093306 (2021).

[55] Z. Yu, Y. Xia, Y. Guo, and J. Lin, Modulation of turbulence intensity by heavy finite-size particles in upward channel flow, J. Fluid Mech. **913**, A3 (2021).